Different emotional states engage distinct descending pathways from the prefrontal cortex

Pan Xu[1,7 #], Gyeongah Park[2 #], Xiaoqian Sun[3 #], Qian Ge[2 #], Zhen Jin[2], Chien-Hsien Lai[1], Xiaojie Liu[4], Qingsong Liu[4], Rahul Simha[3], Chen Zeng[5], Jianyang Du[2,6 *], Hui Lu[1 *]

[1]Department of Pharmacology and Physiology, School of Medicine and Health Sciences, The George Washington University, Washington, DC 20037, USA
[2]Department of Anatomy and Neurobiology, University of Tennessee Health Science Center, Memphis, TN 38163, USA.
[3]Department of Computer Science, School of Engineering and Applied Science, The George Washington University, Washington, DC 20037, USA
[4]Department of Pharmacology and Toxicology, Medical College of Wisconsin, Milwaukee, WI 53226, USA
[5]Department of Physics, Columbia College of Art and Sciences, The George Washington University, Washington, DC 20037, USA
[6]Neuroscience Institute, University of Tennessee Health Science Center, Memphis, TN, United States.
[7]Present address: Medical Science and Technology Innovation Center, Shandong First Medical University & Shandong Academy of Medical Sciences, Jinan, Shandong 250000, China

*Corresponding author: Jianyang Du, Ph.D., jdu15@uthsc.edu; Hui Lu, Ph.D., huilu@email.gwu.edu;

# These authors contributed equally to this work.

Author contributions

H.L. and J.D. conceived the project. H.L., J.D., P. X., G.P., Q.G., Z.J. designed the experiments. P. X. performed the in vivo Ca^{2+} experiments. X.S., C.L, R. S. and C.Z. performed imaging data analysis. Q.G. and Z.J., performed the behavior experiments. Z.J. performed the mouse surgery experiment. G.P. performed optogenetics and patch-clamp experiments and data analysis. X.L. and Q.L. performed histology. H.L. and J.D. wrote the manuscript. All authors reviewed and edited the manuscript.

Declaration of interests:

The authors declare no competing financial interests.

Classification: Biological Sciences/Neuroscience

Keywords: Emotion regulation, Medial prefrontal cortex, Basal lateral amygdala, Nucleus accumbens, Neural circuits, Emotional processing

ABSTRACTS

Emotion regulation, essential for adaptive behavior, depends on the brain's capacity to process a range of emotions. Current research has largely focused on individual emotional circuits without fully exploring how their interaction influences physiological responses or understanding the neural mechanisms that differentiate emotional valence. Using in vivo calcium imaging, electrophysiology, and optogenetics, we examined neural circuit dynamics in the medial prefrontal cortex (mPFC), targeting two key areas: the basal lateral amygdala (BLA) and nucleus accumbens (NAc). Our results demonstrate distinct activation patterns in the mPFC→BLA and mPFC→NAc pathways in response to social stimuli, indicating a mechanism for discriminating emotions: increased mPFC→BLA activity signals anxiety, while heightened mPFC→NAc responses are linked to exploration. Additionally, chronic emotional states amplify activity in these pathways—positivity enhances mPFC→NAc, while negativity boosts mPFC→BLA. This study sheds light on the nuanced neural circuitry involved in emotion regulation, revealing the pivotal roles of mPFC projections in emotional processing. Identifying these specific circuits engaged by varied emotional states advances our understanding of emotional regulation's biological underpinnings and highlights potential targets for addressing emotional dysregulation in psychiatric conditions.

Significance statement

While existing circuitry studies have underscored the significance of emotional circuits, the majority of research has concentrated on individual circuits. The assessment of whether and

how the balance among multiple circuits influences overall physiological outcomes is often overlooked. This study delves into the neural underpinnings of emotion regulation, focusing on how positive and negative valences are discriminated and managed. By examining the specific pathways from the medial prefrontal cortex (mPFC) to key emotional centers—the basal lateral amygdala (BLA) for negative valence and the nucleus accumbens (NAc) for positive one—we uncovered a novel dual-balanced neural circuit mechanism that enables this essential aspect of human cognition.

Introduction

Emotions, in their intricate complexity, weave the fabric of our psychological experiences, oscillating between the poles of joy and despair. This rich emotional tapestry raises a fundamental question: how does our brain navigate the nuanced spectrum of emotions with positive or negative valence to orchestrate appropriate responses? While existing circuitry studies have underscored the significance of emotional circuits, the majority of research has concentrated on individual circuits. The assessment of whether and how the balance among multiple circuits influences overall physiological outcomes is often overlooked. Unfortunately, this scenario appears to mirror real situations due to the intricate interconnections within the tightly related brain networks. Thus, the objective of this study is to elucidate the underlying mechanism governing the balance among distinct emotional circuits.

We initiated our journey by examining the projections of the PFC, a maestro conducting the symphony of our emotional life through its descending pathways (1-4). The descending pathways from the PFC refer to the neural connections that originate from the PFC and project to other regions in the brain, allowing the PFC to exert regulatory influence on their activity. These pathways provide a top-down modulation of emotional processing in other brain regions, allowing the PFC to regulate emotional responses in a flexible and context-dependent manner (5). The descending pathways from the PFC are involved in several key mechanisms of emotion regulation, which include modulating subcortical regions, cognitive reappraisal, attentional control, working memory, and feedback regulation (6-8). For instance, the PFC sends descending pathways to subcortical regions, such as the amygdala, nucleus accumbens, hypothalamus, lateral habenula and periaqueductal gray, which are involved in emotional

processing (4, 9-12). These pathways allow the PFC to modulate the activity of these subcortical regions, influencing their processing of emotional information and subsequent emotional responses. Additionally, the PFC's descending pathways are involved in cognitive reappraisal, a strategy used to regulate emotions by reinterpreting the meaning of a situation (8). A remarkable fact is that individual projections from the PFC do not function in isolation; rather, they work together as a network to govern overall emotional output. However, the interplays among the mPFC projections remain largely unknown.

To explore this question, we focused our research on two distinct descending pathways from the mPFC that target the basolateral amygdala (BLA) and the Nucleus Accumbens (NAc). These pathways are recognized for their vital roles in emotional processing, yet to date, they have not been thoroughly studied. Notably, the amygdala plays an essential part in the creation and processing of emotional memories, especially those linked to negative emotions like fear and anxiety (12-14). On the other hand, the NAc is a critical brain region involved in the regulation of *positive* emotions, stress modulation, reward processing, and motivation (11, 15, 16). Recent study shows that the intriguing interplay between social and spatial information within the mPFC to NAc pathway may play a pivotal role in shaping social behavior through the facilitation of social-spatial learning(17). To delve into the encoding mechanisms of different emotional states within these pathways, we adopted various approaches, including in vivo calcium (Ca^{2+}) imaging, optogenetics, electrophysiological recordings, and behavioral assays. Notably, we employed a social competition behavioral paradigm to naturally induce either positive or negative emotional states in mice, followed by the investigation of synaptic alterations within these descending pathways. These techniques allowed us to investigate how projection-defined mPFC neurons projecting to the BLA (mPFC→BLA) and NAc (mPFC→NAc) contribute to the encoding of various emotional states. Our findings revealed distinct circuit dynamics and plasticity patterns between these two ensembles, which are closely associated with different emotional states in mice.

Results

The mPFC→NAc neurons, as opposed to mPFC→BLA neurons, encode emotional information associated with social preference.

The social behavior can effectively reflect various emotional states in individuals(18) and is encoded by the mPFC neuron ensembles with distinct activity patterns(19). We thus investigated whether distinct activity patterns are exhibited by mPFC→BLA and mPFC→NAc neurons, correlating with different social states, using adult female wildtype mice at the age of ~20 weeks. To distinguish between these two types of neurons (mPFC→BLA and mPFC→ NAc), we employed retrograde AAV viruses carrying genes encoding the Ca^{2+} indicator GCaMP6m, delivering them to the BLA and NAc, respectively (**Fig. 1A**). This allowed for the infection of mPFC neurons projecting to either of these regions, leading to GCaMP6 expression in the soma situated in the mPFC (**Fig. 1B**). In vivo Ca^{2+} imaging was conducted on mPFC→ BLA and mPFC→NAc neurons using a portable miniaturized microscope (**Fig. 1C**). The activity of individual neurons was continuously monitored throughout the behavioral assays.

The social test was conducted using a three-chamber apparatus (**Fig. 1D**). The two end chambers were equipped with either another mouse or an object. The subject mouse underwent a 10-minute acclimation phase in the central 45 cm chamber, with the 10 cm end compartments empty. Subsequently, three ten-minute testing sessions (S1, S2, and S3) were conducted, each involving different stimuli in the end chambers to assess interaction. Utilizing automated tracking software, the time spent within the "sniffing zone" was measured. Notably, the mice exhibited a preference for interacting with fellow mice over objects in sessions 1 and 2. In session 2, this preference gap narrowed due to the relocation of objects. Remarkably, during session 3, wherein the choice was between two mice, the mice displayed a greater inclination to explore the new mouse (**Fig. 1E**). These findings collectively signify a normal level of sociability as observed in the three-chamber test.

To explore the neural activity associated with distinct social states, we closely monitored the excitatory mPFC→BLA and mPFC→NAc neurons within the prelimbic region of the mPFC. Surprisingly, both the mPFC→BLA and mPFC→NAc neurons exhibited little discernible difference in their Ca^{2+} transient rate and amplitude while the mice interacted with the social stimulus (mouse 1, M1) and the nonsocial stimulus (object, O) (**Fig.1F** and **SI Appendix, Fig. S1**). Likewise, no significant variation emerged during session 3. Given that interactions with

social and nonsocial stimuli are known to induce differing emotional states, as reflected in social preference, our findings suggested that the neural encoding of these distinct emotional states was not reliant on the overall firing rate and amplitude of the mPFC→BLA and mPFC→NAc neurons.

Next, we analyzed the ability of these two groups of neurons to convey information through coactivity patterns (20). Functional correlations (coactivity) within the circuit can be identified using Pearson correlation coefficients, and pattern decorrelation serves to clarify overlapping activity patterns. This mechanism is akin to how the olfactory bulb distinguishes closely related odorants based on minor structural variations (21-23). In a previous study, we demonstrated that pattern decorrelation of mPFC excitatory circuit neuronal activities is indispensable for social preference (24). This led us to contemplate whether differences existed between the mPFC→BLA and mPFC→NAc neurons. We thus calculated the pairwise Pearson correlation coefficients of neuronal activities specifically during the interaction with the social or object stimulus (**Fig. 1G**). The pairwise correlation coefficients for different stimuli across the recorded mPFC→BLA and mPFC→NAc neurons from all mice exhibited a distribution around zero, albeit with varying widths (**Fig. 1G**). Intriguingly, we observed a significant pattern decorrelation only within the mPFC→NAc neurons, evident by the full-width at half maximum (FWHM) of the correlation distribution being lower for the more-attractive stimuli in each session. Conversely, such a phenomenon was not observed in the mPFC→BLA neurons (**Fig. 1G and 1H**). The heightened pattern decorrelation of neuronal activity in the mPFC→NAc neurons during social interactions strongly suggests their pivotal role in encoding different emotional states and guiding social preference in mice.

The mPFC→NAc and mPFC→BLA neurons exhibit contrasting correlations with emotional states of opposite valence.

We then performed the open field test, a widely employed behavioral assay in rodent research for assessing exploratory and anxiety-like behaviors (**Fig. 2A**). This test leverages the inherent conflict rodents experience between their desire to explore new environments and their instinctive aversion to exposed spaces. We monitored and recorded the mouse's movements

and actions over a 10-minute period, specifically tracking time spent in the center versus the corner, wall-sniffing, and grooming. These behaviors observed during the open field test-spending time in corners, the center area, grooming, and sniffing walls—offer valuable insights into their emotional states. Typically, mice in corners exhibit lower anxiety levels, suggesting a sense of security. Conversely, exposure to the center area may induce higher anxiety due to increased exposure and reduced safety compared to the arena's edges or corners. Grooming behaviors can signal stress relief or comfort, while wall-sniffing reflects sensory exploration and vigilance, possibly indicating curiosity, cautious exploration, or heightened alertness (25, 26). Our findings demonstrate that mice consistently spend significant time in corners during the 10-minute session. Additionally, they allocate around 10% of the time to the center area or grooming, and approximately 5% of the time to wall-sniffing (**Fig. 2B**). The sniffing time is excluded from the corner-dwelling time if sniffing takes place in the corner area.

During our observation of mPFC→BLA and mPFC→NAc neuron activity, we determined that the collective averaged amplitude and transient rate of these neurons did not exhibit discernible differences while the mice were situated in the center or corner (**SI Appendix, Fig. S2A and S2B**). To delve deeper, we conducted a Principal Component Analysis (PCA) to assess the population activity pattern linked to various behaviors, encompassing center or corner dwelling, grooming, and sniffing. Interestingly, we noted distinct population activity patterns among both mPFC→BLA and mPFC→NAc neurons corresponding to these behaviors (**SI Appendix, Fig. S2C**). However, when considering these patterns as a collective, they seemed comparable between the two groups. This similarity may arise because averaging neuronal amplitude or transient rate across a population can potentially mask characteristics unique to neurons that encode the emotional states of mice associated with these behaviors. We thus narrowed our focus to neurons that exhibited increased activity during heightened anxiety moments, such as entering the center zone. Termed "center-ON" neurons, these neurons displayed substantial amplitude spikes around the mouse's entry into the center zone, suggesting their response to emotional shifts from low (prior to entry) to high (post-entry into the anxiety-inducing center zone) states (**Fig. 1C and 1D**). Upon comparing the two groups of center-ON neurons, we observed a higher prevalence of center-ON neurons in the mPFC→BLA group compared to the mPFC→NAc group (**Fig. 2E**), suggesting a more pronounced coding of anxiety states by the mPFC→BLA neurons than the mPFC→NAc neurons. When we projected the activity patterns of

these center-ON neurons onto the spatial distribution of the open field arena, both sets of center-ON neurons displayed heightened activity in the center zone. However, the center-ON neurons in the mPFC→NAc population exhibited increased activity during sniffing as well, which was not observed in the mPFC→BLA population (**Fig. 2F**). This finding implies that these two sets of center-ON neurons serve distinct roles in encoding the emotional states of the mice. Specifically, the mPFC→NAc neurons appear to be more involved in positive emotional states associated with exploration, while the mPFC→BLA neurons are more associated with negative emotional states related to anxiety. To reinforce this notion, we conducted the PCA exclusively on the center-ON neuron populations (**Fig. 2G**). Intriguingly, the activity patterns of the mPFC→BLA pathway's center-ON neurons exhibited a substantial degree of overlap across behaviors, except for the patterns corresponding to center-dwelling time. Conversely, the activity patterns of the mPFC→NAc pathway's center-ON neurons demonstrated distinct separations for each behavioral state (**Fig. 2G**), further supporting the divergent roles of these neural populations.

To further investigate if the mPFC→BLA and the mPFC→NAc neurons play diverged roles in encoding mouse's emotion states, we had the same mice perform another behavioral assay for anxiety, the Elevated Plus Maze (EPM) test one day after the open field test (**SI Appendix, Fig. S3A**). During the EPM test, mice that venture onto the open arms of the maze are likely experiencing higher levels of anxiety or fear as the open arms are exposed and elevated, making them less secure and potentially more threatening to the mice. Mice that prefer to stay in the closed arms of the maze are likely to display lower levels of anxiety and greater comfort as the closed arms provide a sheltered and enclosed environment, which is perceived as safer by the mice. We observed that mice spent significantly more time in the closed arms of the EPM test, avoiding the open arms that generally induce higher anxiety. Individual mice exhibited a preference for either one of the open arms (referred to as open-P arm) or one of the closed arms (referred to as closed-P arm), avoiding the other pair of arms (referred to as open-NP or closed-NP arm). The preference appeared randomly and did not correlate with the location of the arms (i.e. left or right arm). Interestingly, mice tended to spend the majority of their time in the closed-P arm, akin to a home base, even though both closed arms were designed to provide a low-anxiety environment (**SI Appendix, Fig. S3B**).

We observed that the recorded neuronal populations of mPFC→BLA and mPFC→NAc pathways displayed elevated averaged amplitude and transient rate in the open arms compared to the closed arms, indicating their response to the anxiety-inducing open-arm environment. However, the overall activity patterns of neurons in these pathways did not show pronounced differences (**SI Appendix, Fig. S3C**), consistent with findings from the open field test (**SI Appendix, Fig. S1**). Our subsequent analysis focused on the "center-ON" neurons identified in the open field test, examining their activity during distinct behavioral states in the EPM (**Fig. 2H and 2I**). Notably, the center-ON neurons in the mPFC→BLA pathway exhibited significantly higher activity when mice entered (**Fig. 2J**) and spent time in the open arms (**Fig. 2K)** compared to the closed arms, in comparison to the center-ON neurons in the mPFC→NAc pathway. The Ca^{2+} transient rate in the mPFC→BLA neurons was notably greater than that in the mPFC→ NAc neurons when mice were in the open arms (**Fig. 2K**). The difference is most noticeable when mice are in the open-NP arm, likely due to its unfamiliarity causing increased anxiety. These findings further support our observations from the open field test, highlighting the more prominent role of mPFC→BLA neurons in responding to mouse emotional states related to anxiety.

The mPFC→NAc and the mPFC→BLA neurons were manipulated distinctly by chronic emotional states.

Demonstrating the mPFC→NAc and mPFC→BLA neurons as encoding acute positive and negative emotions, respectively, led us to question whether these pathways could also be influenced by naturally induced emotional states. Competitions, such as winning or losing, are effective natural means to induce opposite emotions. The social dominance tube test, commonly used to evaluate social hierarchy and aggression in rodents, serves as an ideal method for natural emotion induction. It involves placing two mice in a clear narrow tube to observe their interactions as they navigate toward opposite ends (27-31). Repeated daily over a week, this procedure often results in mice adopting consistent winner or loser roles, potentially leading to sustained positive or negative emotional states.

To verify if the tube test genuinely altered emotional states, littermate mice underwent an open field test both before and after the tube test (**Fig. 3A**). Initially, there was no difference in the travel distance or time spent in the center of the open field arena between winner and loser mice (**Fig. 3B**). Post-tube test, travel distances remained unchanged, suggesting that mobility was not affected by induced emotions. However, loser mice spent significantly less time in the center, indicating heightened anxiety and successful negative emotion induction. In contrast, winners' time in the center remained unchanged, implying their anxiety levels remained normal (**Fig. 3C and 3D**). Furthermore, to determine if the tube test could evoke positive emotions in winner mice, their sociability was assessed before and after the test because positive emotion (such as the pleasure from winning) would enhance sociability (**Fig. 3E**). Initially, both the winner and loser mice showed a standard preference for interacting with a live mouse over an inanimate object, and a new mouse over a familiar one (**Fig. 3F**). After the tube test, winners displayed a higher sociability index towards social mice and a tendency for greater interest in new mice. In contrast, losers almost entirely lost their social preference, underscoring the induction of negative emotions (**Fig. 3G and 3H**). These findings confirm that the repeated competitions in the tube test successfully induced distinct positive and negative emotions in the winner and loser mice, respectively.

Next, we compared the synaptic strength in the mPFC→NAc and mPFC→BLA circuits following emotion induction via the repeated tube test. To activate these circuits, we used AAV-mediated expression of channelrhodopsin-2 (ChR2) for selective stimulation of prelimbic (PL) neurons in the NAc and BLA using blue light. ChR2-EYFP expression was verified in the PL, with terminal expression in the NAc and BLA (**Fig. 4A and 4B**). Following the establishment of stable social rankings through the tube test (**Fig. 4C**), we recorded from brain slices containing the NAc or BLA. Blue light application confirmed ChR2 activation, triggering inward currents and action potentials in both winner and loser mice (**Fig. 4D and 4H**). In the mPFC→NAc pathway, blue light stimulation evoked larger excitatory postsynaptic currents (EPSCs) in winner mice compared to losers (**Fig. 4E**), despite similar paired-pulse ratios (PPRs) in both groups (**Fig. 4F and 4G**). This suggests stronger synaptic transmission in winners' mPFC→NAc circuits. Conversely, in the mPFC→BLA pathway, loser mice exhibited larger EPSCs and significantly higher PPRs than winners (**Fig. 4E-4G**), indicating stronger synaptic transmission in losers'

mPFC→BLA circuits. Additionally, the AMPA/NMDA receptor-mediated EPSC ratio was higher in winners' mPFC→NAc circuits and losers' mPFC→BLA circuits (**SI Appendix, Fig. S4**).

Importantly, we observed no significant differences in synaptic strength between winner and loser mice within the mPFC region. The correlation between the light intensity and the normalized amplitude of blue light-induced current showed no variance between the winner and loser groups during light stimulation and recordings in the PL region of the mPFC (**SI Appendix, Fig. S5A-S5C**). Furthermore, the induction of emotional states did not alter the excitability of mPFC neurons; this is evident from the consistent relationship between light stimulation frequency and the number of action potentials induced across mPFC neurons from both winner and loser mice (**SI Appendix, Fig. S5D and S5E**). Consequently, it appears that the induction of emotion specifically affects the descending pathway from the mPFC, rather than the neuronal activity within the mPFC itself. Overall, our findings reveal that chronic positive emotions correlate with enhanced synaptic strength in the mPFC→NAc pathway, while chronic negative emotions are linked to increased synaptic strength in the mPFC→BLA pathway. These outcomes underscore the divergent modulation of mPFC inputs to the BLA and NAc by positive and negative emotional states, further illuminating the distinct roles of these circuits in encoding emotional states with opposite valence.

Discussion

In this study, we investigated the functional roles of two distinct mPFC neuronal pathways projecting to the BLA and the NAc, respectively, in the regulation of emotional states and behavior in mice. The results reveal intriguing insights into the differential modulation of these pathways in response to anxiety-inducing environments, exploration, and chronic emotional states.

Our findings illuminate distinct neural responses based on the projection targets of mPFC neurons. The mPFC neurons projecting to the NAc displayed a discernible activity pattern, particularly during exploration. These neurons exhibited activity profiles enabling discrimination between social and non-social cues, suggesting their involvement in processing reward-related

information and exploration behavior (32, 33). This functional dissociation highlights the pivotal role of the mPFC→NAc pathway in mediating positive emotional states associated with curiosity and exploration. Our investigation into the temporal correlation of neuronal activities in response to social and object stimuli has illuminated a distinct pattern of decorrelation within the mPFC→NAc neurons. This phenomenon underscores their specialized role in encoding diverse emotional states and shaping social preferences in mice. In contrast, notably, mPFC neurons projecting to the BLA exhibited heightened activity in response to anxiety-inducing environments. This observation concurs with prior research highlighting the Amygdala's pivotal role in fear and anxiety processing (34, 35).

In the context of the EPM test, the heightened activities of the mPFC→BLA pathway's center-ON neurons in the open arms corroborate their role in encoding emotions associated with negative anxiety. Conversely, the increased activities of the mPFC→NAc pathway's center-ON neurons during sniffing align with their role in encoding emotions linked to positive exploration. Clearly, the mPFC→BLA and mPFC→NAc neurons utilize distinct activity patterns to represent the mouse's emotional state in these differing zones.

The contrasting patterns of neural activity observed between "center-ON" neurons and the entire neuronal population further underscore the functional diversity within the mPFC→BLA and mPFC→NAc pathways. The broader population of neurons does not exhibit the same selective sensitivity to emotional changes. Instead, their activity appears to be more generalized, without showing the same level of specificity as "center-ON" neurons. This suggests that while the overall activity of these pathways may play a role in modulating emotional states, it is the specialized subset of "center-ON" neurons that provides the most nuanced and accurate representation of emotional shifts, particularly those related to anxiety. In essence, "center-ON" neurons act as a specialized subset that finely tunes the encoding of emotional states in response to specific triggers, such as entry into anxiety-inducing environments. This specialized encoding provides a more detailed and precise understanding of the mice's emotional responses to various situations. On the other hand, the broader neuronal population within these pathways contributes to the overall regulation of emotional responses, albeit in a less specialized manner. Together, these findings underscore the complexity of

neural processing, highlighting the coexistence of specialized and generalized encoding mechanisms within neural circuits.

The comparison between "center-ON" neurons and the broader neuronal population underscores the distinctiveness of these subsets in encoding emotional states. This differentiation provides a deeper insight into the neural circuit mechanisms that govern emotional responses, shedding light on the delicate balance between specialized and generalized encoding mechanisms within the mPFC→BLA and mPFC→NAc pathways. This finding reflects the complexity of neural circuits in processing emotional cues and highlights the importance of distinct pathways in contributing to the multifaceted landscape of emotional responses.

Furthermore, our study has uncovered a fascinating dimension regarding the impact of chronic emotional states on the synaptic strength within these specific neuronal pathways. Notably, we observed that sustained positive emotional states were linked to a reinforcement of synaptic strength in the mPFC→NAc pathway. This aligns well with the NAc's recognized function in processing rewards and promoting positive reinforcement (36, 37). In contrast, chronic negative emotional states correlated with heightened synaptic strength in the mPFC→BLA pathway, further affirming the BLA's pivotal role in processing aversive stimuli and triggering fear responses (38, 39). Significantly, these findings highlight the potential influence of social status on the reward and emotional processing associated with the mPFC descending pathways. This insight offers a critical understanding of the neural circuit mechanisms that govern an animal's emotional state within real-world environments characterized by hierarchical dynamics. However, further research is warranted to delve into the molecular and cellular mechanisms underlying these effects and to ascertain if analogous effects manifest in other brain regions implicated in social status-dependent emotional states.

In summary, our study sheds light on the intricate interplay between distinct mPFC neuronal pathways and their modulation in response to various emotional states and environmental cues. The BLA-projecting neurons appear to play a pivotal role in encoding negative emotional states and responding to anxiety-inducing environments, while the NAc-projecting neurons contribute

to positive emotional states and exploration. These results enhance our knowledge of the neural circuits involved in emotional processing and behavior, setting the stage for more in-depth studies into the intricate mechanisms of emotional regulation and their possible implications for neuropsychiatric disorders.

METHODS AND MATERIALS

Animal care and usage followed NIH Guidelines and received approval from the Institutional Animal Care and Use Committee of George Washington University and The University of Tennessee Health Science Center Laboratory Animal Care Unit.

Experimental Animals

CaMKII-Cre mice with a pure C57BL/6 background were acquired from Jackson Lab (JAX#005359). For excitatory neuron imaging experiments, female CaMKII-Cre mice were bred by mating male CaMKII -Cre mice with female mice from the 129S1/SvlmJ strain (JAX#002448). These experimental CaMKII -Cre mice were used in accordance with the same procedural guidelines. Surgeries were performed on mice at approximately 4 months of age, adhering to the established experimental protocol. Animals were housed in groups of 4 to 5 per cage in a controlled environment with a temperature of 23 ± 1°C, humidity set at 50 ± 10%, and a 12-hour light-dark cycle. Standard mouse chow and water were provided ad libitum.

Virus injection and gradient-index (GRIN) lens implantation

In the context of imaging excitatory neurons, we employed the AAV1-EF1a-flex-GCaMP6m virus acquired from Baylor College of Medicine. Following established protocols (24), CaMKII -Cre mice were anesthetized and securely positioned within a Neurostar stereotaxic frame from Tübingen, Germany. Employing a high-speed rotary stereotaxic drill (Model 1474, AgnTho's AB, Lidingö, Sweden), we conducted a unilateral injection of the retrograde virus into either the left Nucleus Accumbens (NAc) region (anterior-posterior AP: +1.34 mm, medial-lateral ML: -1.1 mm, dorsal-ventral DV: 4.4mm) or Amygdala region (AP: -1.6 mm, M/L: -2.9 mm, DV: 4.5mm) using the Nanojector II system from Drummond Scientific. The injection comprised 300 nL of virus diluted with 300 nL of PBS, administered at a controlled rate of 30 nL/min. Post-injection, the needle was retained in place for an additional 5 minutes to optimize virus diffusion.

Subsequent to viral injection, a precise 1.1 mm-diameter craniotomy was conducted at AP: +1.95 mm, M/L: -0.5 mm coordinates. These values were determined relative to bregma: +1.95 mm AP, -0.35 mm ML, -2.3~-2.5 DV, employing a high-resolution atlas. Following this, a 1-mm diameter GRIN lens (Inscopix, Palo Alto, CA) was progressively lowered into the left PL region (AP: +1.95 mm; ML: ± 0.35 mm; DV: -2.1~-2.3 mm) at a rate of 50 μm/min, situated 0.2 mm above the virus injection site, and then cemented in place using Metabond S380 (Parkell). Subsequently, the mice were allowed to recover on a heating pad and were closely monitored over the ensuing 7 days, during which they received analgesic treatment.

Baseplate attachment

Around three to four weeks post-surgery, we assessed virus expression in the anesthetized mice using a miniaturized microscope from Inscopix, based in Palo Alto, CA. Once GCaMP+ neurons were clearly visible, we proceeded to attach the microscope with a baseplate onto the mouse's skull window. This setup was then gradually lowered to determine the optimal focus plane. Subsequently, the baseplate was securely affixed to the skull using dental cement and covered with a protective cap, while the microscope remained unattached. Ahead of the behavioral tests, the mice were familiarized with the test room environment, during which a dummy microscope was mounted and handled for approximately 5 to 7 days, with sessions lasting 30 to 40 minutes each day.

Selection of animals

Mice were chosen based on specific criteria: for the observation of Ca^{2+} signals in the mPFC, mice were excluded post-hoc if (1) the GRIN lens was positioned outside of the prelimbic cortex, (2) GCamp6 was not expressed within prelimbic areas, (3) significant virus expression was observed outside of the prelimbic region, and (4) the imaging plane was obstructed by blood or debris. In the identification of mPFC neural ensembles, mice exhibiting no center entry behavior were excluded, as the classification was grounded in the neural responses to transitions in location.

Determination of sample size

The sample sizes for behavioral experiments were established following the prevailing standards in behavioral neuroscience research for mice. This approach considers the minimum number of mice needed to detect statistical significance, with an α level of 0.05, and a statistical power of 80% or higher. Our post-hoc analysis demonstrates a statistical power of 85%.

In terms of neuron count, we recorded 11-83 neurons expressing GCaMP6m for the mPFC→BLA group (with an average of 38) and 18-54 for the mPFC→NAc group (with an average of 39). This range was influenced by various factors, including the injected volume of viral GCaMP6m, expression levels, and the efficiency of Cre-mediated recombination. Following the data processing phase, which involved the identification of neurons through principal component and independent component analyses (PCA-ICA), approximately 1-9% of the identified components were identified as artifacts and subsequently excluded. The remaining components were classified as neurons and employed for subsequent analyses.

Behavioral tests

The behavioral tests spanned three consecutive days, maintaining consistent schedules throughout. To ensure cleanliness, the chamber was meticulously cleaned with 70% ethanol between trials. The Topscan behavior analysis system from Clever Sys, VA, was employed to monitor the animals' behaviors. This system also sent a TTL signal at the start of each test to trigger the microscope recording of neural activity.

Modified Three-Chamber (mTC) Test

The mTC test adhered to a previously established protocol (40) with several enhancements. The conventional three-chamber apparatus was transformed into a single open box (45 x 10 x 20 cm) featuring two small removable lateral chambers (10 x 10 x 40 cm). These chambers were separated by thin, spaced metal wires, permitting mice to interact with stimuli. Before the test, the subject mouse underwent a 10-minute habituation period within the open box devoid of stimuli. During testing, an age- and weight-matched, unfamiliar same-sex conspecific (referred to as the first social stimulus, M1) and an inanimate object (non-social stimulus, O) were

randomly placed into the two lateral chambers. Subsequently, the subject mouse was positioned in the center of the open box and allowed to explore freely during a 10-minute testing session. Several behavioral parameters were assessed, including time spent in social interaction, object interaction, the social zone (SZ), the object zone (OZ), the transition zone, and grooming behavior.

Open field (OF) test

The test was modified from a previous report (25). It was conducted in a square box (dimensions: 50 × 50 × 50 cm). The mouse was gently placed in the central field and allowed to explore freely during a 10-minute testing session. Locomotor activity was recorded by a camera. The center is defined as the central 25 cm x 25 cm square area, while the corner is a sector area with a 12.5 cm radius in each corner. Total distance traveled and time spent in each area, sniffing, and grooming behaviors were analyzed.

Elevated plus maze (EPM) test

It was conducted as previously described (41). The EPM apparatus, 40 cm high from the floor, consists of two open arms (35 × 10 cm) and two closed arms (35 × 10 cm), those two parts stretch perpendicular to each other and connect in a center platform (5 cm). Mice were placed in the center zone facing an open arm and allowed to explore the maze freely for 10 min. The time spent in open arms, closed arms, and behaviors of headdipping, sniffing, and grooming were analyzed.

Dominance tube test

The tube test protocol was modified from Wang et al (30). In brief, a clear acrylic tube with a 30 cm length and 2.8 cm inside diameter in which one mouse can pass or backward through the tube fluently but can’t make a U-turn or climb through another mouse. The mice underwent a three-day training in which all mice went through the tube ten times per day, five times from each side without another competitor in the tube. The training procedure allows the mice to adapt to the test procedure and environment. The mice, in a very rare case, cannot be trained and were excluded for further testing. In the testing procedure, tests were conducted in a pair-wise style, and the number of times won by individual animals was recorded to determine the

hierarchical ranking. The mouse who forced its competitor out of the tube was declared the "winner", or dominant in this situation. The mouse that was retreated is then designated the "loser", or subordinate. In most cases, the competition was completed within 2 minutes, or the tests were repeated. The rank is considered stable without ranking change in all mice for at least five consecutive days. Groups were categorized as "non-stable ranking" if they did not form a stable ranking within 2 weeks. We single housed the mice for 5 days and subjected them to a round-robin tube test tournament (three trial per day for 7 trials) to determine social ranking. Twenty-four hours following the last tube test, the mice were subjected to other behavioral tests or in vitro studies, as described in the results.

Behavior data analysis

Behavioral data was meticulously tracked through aerial videography from an overhead perspective utilizing the Topscan behavioral data acquisition software (CleverSys, Reston, VA). This software allowed for the precise tracking and definition of the 2D locations of mice in various areas, including the OF center, corner area, EPM open-P, open-NP, closed-P, closed-NP arms, and mTC social zone, object zone, and middle zone. Additionally, specific behaviors such as sniffing, grooming, head-dipping, and social/object interaction were recognized and quantified by the software.

Ca^{2+} imaging with Miniature microscope

Imaging of freely moving mice was conducted using a head-mounted miniaturized microscope (nVista HD 2.0.4, Inscopix, Palo Alto, CA), as depicted in Fig. 1a, b. This microscope was synchronized with the Topscan system through a TTL pulse, enabling simultaneous acquisition of Ca^{2+} signals and behavioral video. Prior to imaging, the microscope was securely affixed to the mouse's head. The imaging data were obtained at a frame rate of 15 Hz with a resolution of 1024 x 1024 pixels. LED power settings ranged from 0.3 to 1 mW, while gain settings were adjusted to 1 to 2 based on fluorescence intensity. Importantly, each individual mouse utilized the same imaging parameters consistently across all three experimental sessions.

Histology

Recording sites were meticulously validated through histological examination of lesions

created during the lens implantation procedure. Mice were anesthetized via intraperitoneal injection, employing a combination of ketamine (400 mg/kg) and xylazine (20 mg/kg). Following this, transcardial perfusion was conducted using a phosphate buffer solution (PBS), followed by 4% paraformaldehyde (PFA). The brains of the mice, complete with their skulls and baseplates, were post-fixed with 4% PFA for 3 days. Subsequently, the brains were extracted and sectioned into slices measuring 50-100 μm using a vibrating slicer (Vibratome Series 1000, St. Louis, MO). These sections were then mounted onto slides. To label cell nuclei, slides were subjected to incubation and storage in a 1:1000 Hoechst solution in 1x PBS (Invitrogen, Carlsbad, CA). Brain slides were meticulously imaged to precisely determine the placement of the GRIN lens and the extent of viral expression. This imaging process was conducted employing a Confocal Microscope (Zeiss LSM 710, Oberkochen, Germany).

Ca^{2+} image processing

Ca^{2+} images were processed offline using Inscopix Data Processing software (version 1.3.1). In brief, frames collected within a single day were concatenated into a stack and subsequently subjected to preprocessing, spatial filtering, and motion correction. To normalize the Ca^{2+} signal, the average projection of the filtered video was established as the background fluorescence (F_0). Instantaneous normalized Ca^{2+} fluorescent signals ($\Delta F/F$) was calculated according to the formula, $(\Delta F/F)_i=(F_i-F_0)/F_0$, where i represents each frame. Individual cells were then identified using the principal component and independent component (PCA-ICA) analyses with no spatial or temporal down-sampling. Regions of interest (ROI) were selected based on signal and image criteria, with any components that did not correspond to single neurons being discarded.

Time-stamped traces of neurons were exported into data files formatted for custom-written Python scripts used for subsequent analysis. Ca2+ transients (events) were identified for each cell using a peak-finding algorithm, and frequency (transient rate) and amplitude ($\Delta F/F$) data were processed using custom-written scripts. When analyzing frequency or amplitude changes in response to mouse behavior or location, frames of image and behavioral data were aligned and marked with corresponding behavioral event labels. For neural activity normalization, we employed the min-max normalization method to scale values between 0 and 1. In this method, the maximum neuron activity value was transformed into 1, while all other values were scaled to decimals between 0 and 1 using the equation: $z_i = \frac{x_i - min_{(x)}}{max_{(x)} - min_{(x)}}$, where x=(x1,x2,...,xn)

represents an array of neuron frequency or amplitude values, and z_i denotes the normalized value.

Identification of location-modulated neural ensembles

To identify location-modulated neural ensembles in each session, we assessed each neuron's response preference to a specific location exploration. Initially, we computed the actual similarity (Sa) between the Ca^{2+} trace vectors (c_k) and behavior events (b), using the formula: $2b \cdot c_k/(|b|^2 + |c_k|^2)$ (19). Then, the behavior vector was subjected to random shuffling to compute a new similarity (S) with a neural trace for a given neuron. This shuffling process was repeated 5000 times, generating an S distribution histogram. Neurons were classified as ON neurons if their Sa values exceeded the 99.95th percentile of the S distribution.

Following neuron identification, we calculated the proportions of different location-modulated ON neurons for each mouse. Simultaneously, the transient rate and amplitude of these neuron ensembles were computed for each mouse in each paradigm.

Neuron alignment between tests

To identify and compare the same neurons across tests conducted on different days, thus enabling cross-test comparisons, we implemented a global alignment procedure. Initially, we reconstructed neuron distribution images based on their pixel locations and shapes. Subsequently, we converted each neuron image into a vector format and assessed their similarity using cosine similarity, as indicated by the formula below. The two parameters, degree of rotation (A) and pixel shift (B), were iteratively adjusted to maximize the cosine similarity of image vectors between tests. Given that the images from all three tests were collected under identical settings, the scale for the neuron images remained constant and did not require adjustment. Through this multi-start method, we achieved the global optimal solution for the parameters. Ultimately, we determined the number of overlapping neuron images across tests, which was then used for subsequent comparative analyses.

$$\text{Similarity} = \cos(\theta) = \frac{A \cdot B}{\| A \| \| B \|}$$

Optogenetics and patch-clamp recording

Viral injection for optogenetics

We stereotaxically injected an AAV_2-CaMKIIα-hChR2(H134R)-EYFP (UNC virus core, 0.5 μl of 1.00 E13 viral genomes/ml) into mPFC bilaterally (relative to bregma: +1.9 mm AP; ±0.3 mm ML; -2.0 mm DV) using a Hamilton microsyringe (Model 1701N) and a WPI microsyringe pump mounted to a KOPF Model 940 Small Animal Stereotaxic Instrument.

After viral injection, mice were recovered for 2 weeks to allow for the AAVs' efficacy. We then retrograde tracing from the mPFC to the NAc and BLA in brain slices. After euthanasia using 2% isoflurane, the mice underwent transcardial perfusion with 4% PFA to fix the entire brain. After a 6-hour fixation period, 50 μm coronal slices, encompassing the mPFC, NAc, and BLA, were dissected using a vibratome (Leica VT-1000S) and collected in ice-cold PBS. These sections were transferred onto gelatin-coated slides (Thermo Fisher Scientific) and mounted onto cover slides (Electron Microscopy Sciences). Nuclei were labeled using Gold antifade reagent with DAPI (Invitrogen). Fluorescence images were captured and visualized at 10x and 20x magnification under a Leica microscope (DMRXA2, Leica Microsystems) equipped with a digital camera and imaging software.

Brain slice preparation.

The patch clamp test was conducted following the completion of the tube test. Mice were anesthetized with 2% isoflurane and subsequently decapitated. The brain skull was swiftly removed and immersed in an ice-cold cutting solution composed of the following concentrations (in mM): 205 sucrose, 5 KCl, 1.25 NaH_2PO_4, 5 $MgSO_4$, 26 $NaHCO_3$, 1 $CaCl_2$, and 25 glucose; with an osmolarity of 300-320 mOsm. The brain was then sliced into 300-μm coronal sections using a vibratome (Leica VT-1000S), encompassing the mPFC, NAc, and BLA.

Post-sectioning, slices were maintained in a normal artificial cerebrospinal fluid (ACSF) solution for whole-cell recording, containing the following concentrations (in mM): 115 NaCl, 2.5 KCl, 2 $CaCl_2$, 1 $MgCl_2$, 1.25 NaH_2PO_4, 17 glucose, 25 $NaHCO_3$; with an osmolarity of 280-300 mOsm. The slices were bubbled with 95% O_2 / 5% CO_2 for one hour at ambient temperature (22 ± 3°C). Whole-cell patch-clamp recordings were conducted by placing the slices in a submerged

recording chamber and perfusing them with ACSF at a rate of 1 ml/min.

Patch-clamp recording

The pipette solution for EPSC recordings contained (in mM): 145 Cs-methanesulfonate (Cs-SO_3CH_3), 8 NaCl, 1 $MgCl_2$, 0.38 $CaCl_2$, 1 Cs-EGTA, and 10 HEPES (mOsm 280 - 300, adjusted to pH 7.25 with CsOH). For action potential recordings, $CsSO_3CH_3$ was replaced by K-SO_3CH_3. The pipette resistance was 8-10 M ohm. Brain slices were recorded through an Axon Instruments Multiclamp 700B amplifier, sampled at 10 kHz, and digitized with a Digidata 1440A (Molecular Device software). The cell morphology was identified under an Olympus BX51 fluorescence microscope. 100 μM picrotoxin was included in the ACSF throughout the recording.

A blue light pulse (PlexBright LED, 470nm) was utilized to activate mPFC fibers expressing ChR2. To validate the expression of ChR2 in the mPFC, inward current in voltage-clamp recording was assessed at -80 mV for 1 second, with a light intensity of 1 μW. Furthermore, action potential firing was examined in current clamp mode at frequencies of 5, 10, and 20 Hz, induced by a 1 ms light pulse with an intensity of 1 μW.

To elicit synaptic responses in the NAc and BLA through light pulses targeting mPFC fibers, slices were illuminated at 30-second intervals, with a short duration of 1-5 ms for NAc neurons and 1-10 ms for BLA neurons. EPSCs were induced by incrementally increasing light intensity (1, 2, 5, and 10 μW) at a holding potential of -80 mV, normalized by dividing by the response at 10 μW. PPR responses at 50 and 75 ms intervals were measured at an intensity of 1 μW, and the amplitude of the second response was divided by that of the first response. To determine the AMPA/NMDA current ratio, current responses were recorded at a holding potential of –70 mV (AMPA) and +40 mV (NMDA), with an intensity of 2 μW.

Statistics

All statistical analyses were performed using SPSS (version 24, IBM, Armonk, NY), Excel (Microsoft, Redmond, WA), and Python custom scripts. Since all the data could pass the normal distribution test (D'Agostino and Pearson), a two-tailed paired or unpaired t-test was applied for

two-group comparison, whereas one-way ANOVA and multiple comparison test (Tukey) was used for multiple-group comparison. For multiple-factors comparison, two-way RM ANOVA was used, followed by Bonferroni-corrected post hoc comparisons. Statistical significance was taken as $^{*}P < 0.05$, $^{**}P < 0.01$. All data are represented as mean ± SEM unless otherwise specified.

Data availability

All data that support the findings in this study and the code used to analyze the data are available upon reasonable request.

Acknowledgments

This work was supported by the NIH grant R01NS118197, and the George Washington University 2018-2023 Cross-Disciplinary Research Fund to H. L. and R.S. / C. Z. The National Institutes of Mental Health (1R01MH113986), the Cystic Fibrosis Foundation (002544I221), and the University of Tennessee Health Science Center start-up fund to J.D.

References

1. M. V. Chafee, S. R. Heilbronner, Prefrontal cortex. *Curr Biol* **32**, R346-R351 (2022).
2. D. R. Euston, A. J. Gruber, B. L. McNaughton, The role of medial prefrontal cortex in memory and decision making. *Neuron* **76**, 1057-1070 (2012).
3. E. K. Miller, The prefrontal cortex and cognitive control. *Nat Rev Neurosci* **1**, 59-65 (2000).
4. H. Barbas, S. Saha, N. Rempel-Clower, T. Ghashghaei, Serial pathways from primate prefrontal cortex to autonomic areas may influence emotional expression. *BMC Neurosci* **4**, 25 (2003).
5. A. Etkin, T. Egner, R. Kalisch, Emotional processing in anterior cingulate and medial prefrontal cortex. *Trends Cogn Sci* **15**, 85-93 (2011).
6. T. J. Buschman, E. K. Miller, Top-down versus bottom-up control of attention in the prefrontal and posterior parietal cortices. *Science* **315**, 1860-1862 (2007).
7. S. B. J. Koch, R. B. Mars, I. Toni, K. Roelofs, Emotional control, reappraised. *Neurosci Biobehav Rev* **95**, 528-534 (2018).
8. T. Steward *et al.*, Dynamic Neural Interactions Supporting the Cognitive Reappraisal of Emotion. *Cereb Cortex* **31**, 961-973 (2021).
9. R. Dampney, Emotion and the Cardiovascular System: Postulated Role of Inputs From the Medial Prefrontal Cortex to the Dorsolateral Periaqueductal Gray. *Front Neurosci* **12**, 343 (2018).

10. Z. Fan *et al.*, Neural mechanism underlying depressive-like state associated with social status loss. *Cell* **186**, 560-576 e517 (2023).

11. S. B. Floresco, The nucleus accumbens: an interface between cognition, emotion, and action. *Annu Rev Psychol* **66**, 25-52 (2015).

12. C. D. Salzman, S. Fusi, Emotion, cognition, and mental state representation in amygdala and prefrontal cortex. *Annu Rev Neurosci* **33**, 173-202 (2010).

13. A. Adhikari *et al.*, Basomedial amygdala mediates top-down control of anxiety and fear. *Nature* **527**, 179-185 (2015).

14. W. Z. Liu *et al.*, Identification of a prefrontal cortex-to-amygdala pathway for chronic stress-induced anxiety. *Nat Commun* **11**, 2221 (2020).

15. W. A. Carlezon, Jr., M. J. Thomas, Biological substrates of reward and aversion: a nucleus accumbens activity hypothesis. *Neuropharmacology* **56 Suppl 1**, 122-132 (2009).

16. C. W. Stevenson, A. Gratton, Basolateral amygdala modulation of the nucleus accumbens dopamine response to stress: role of the medial prefrontal cortex. *Eur J Neurosci* **17**, 1287-1295 (2003).

17. M. Murugan *et al.*, Combined Social and Spatial Coding in a Descending Projection from the Prefrontal Cortex. *Cell* **171**, 1663-1677 e1616 (2017).

18. D. K. a. A. M. Kring, Emotion, Social Function, and Psychopathology. *Review of General Psychology* **2**, 320-342 (1998).

19. B. Liang *et al.*, Distinct and Dynamic ON and OFF Neural Ensembles in the Prefrontal Cortex Code Social Exploration. *Neuron* **100**, 700-714 e709 (2018).

20. N. A. Frost, A. Haggart, V. S. Sohal, Dynamic patterns of correlated activity in the prefrontal cortex encode information about social behavior. *PLoS Biol* **19**, e3001235 (2021).

21. M. R. Cohen, J. H. Maunsell, Attention improves performance primarily by reducing interneuronal correlations. *Nat Neurosci* **12**, 1594-1600 (2009).

22. R. W. Friedrich, M. T. Wiechert, Neuronal circuits and computations: pattern decorrelation in the olfactory bulb. *FEBS Lett* **588**, 2504-2513 (2014).

23. J. F. Mitchell, K. A. Sundberg, J. H. Reynolds, Spatial attention decorrelates intrinsic activity fluctuations in macaque area V4. *Neuron* **63**, 879-888 (2009).

24. P. Xu *et al.*, Pattern decorrelation in the mouse medial prefrontal cortex enables social preference and requires MeCP2. *Nat Commun* **13**, 3899 (2022).

25. L. Prut, C. Belzung, The open field as a paradigm to measure the effects of drugs on anxiety-like behaviors: a review. *Eur J Pharmacol* **463**, 3-33 (2003).

26. R. N. Walsh, R. A. Cummins, The Open-Field Test: a critical review. *Psychol Bull* **83**, 482-504 (1976).

27. V. K. Adam C. Nelson, Eric Vaughn, Jeshurun A. Gnanasegaram, Nimrod D. Rubinstein, Venkatesh N Murthy, Catherine Dulac, Molecular and Circuit Architecture of Social Hierarchy. *bioRxiv* https://doi.org/10.1101/838664 (2019).

28. Z. Fan *et al.*, Using the tube test to measure social hierarchy in mice. *Nat Protoc* **14**, 819-831 (2019).

29. L. Kingsbury *et al.*, Correlated Neural Activity and Encoding of Behavior across Brains of Socially Interacting Animals. *Cell* **178**, 429-446 e416 (2019).

30. F. Wang *et al.*, Bidirectional control of social hierarchy by synaptic efficacy in medial prefrontal cortex. *Science* **334**, 693-697 (2011).

31. T. Zhou *et al.*, History of winning remodels thalamo-PFC circuit to reinforce social dominance. *Science* **357**, 162-168 (2017).

32. K. C. Berridge, M. L. Kringelbach, Pleasure systems in the brain. *Neuron* **86**, 646-664 (2015).

33. S. Ikemoto, Dopamine reward circuitry: two projection systems from the ventral midbrain to the nucleus accumbens-olfactory tubercle complex. *Brain Res Rev* **56**, 27-78 (2007).

34. M. Davis, The role of the amygdala in fear and anxiety. *Annu Rev Neurosci* **15**, 353-375 (1992).

35. J. E. LeDoux, Emotion circuits in the brain. *Annu Rev Neurosci* **23**, 155-184 (2000).

36. T. W. Robbins, B. J. Everitt, Neurobehavioural mechanisms of reward and motivation. *Curr Opin Neurobiol* **6**, 228-236 (1996).

37. W. Schultz, Behavioral dopamine signals. *Trends Neurosci* **30**, 203-210 (2007).

38. E. A. Phelps, J. E. LeDoux, Contributions of the amygdala to emotion processing: from animal models to human behavior. *Neuron* **48**, 175-187 (2005).

39. P. Tovote, J. P. Fadok, A. Luthi, Neuronal circuits for fear and anxiety. *Nat Rev Neurosci* **16**, 317-331 (2015).

40. E. Lee *et al.*, Enhanced Neuronal Activity in the Medial Prefrontal Cortex during Social Approach Behavior. *J Neurosci* **36**, 6926-6936 (2016).

41. A. A. Walf, C. A. Frye, The use of the elevated plus maze as an assay of anxiety-related behavior in rodents. *Nat Protoc* **2**, 322-328 (2007).

Fig. 1

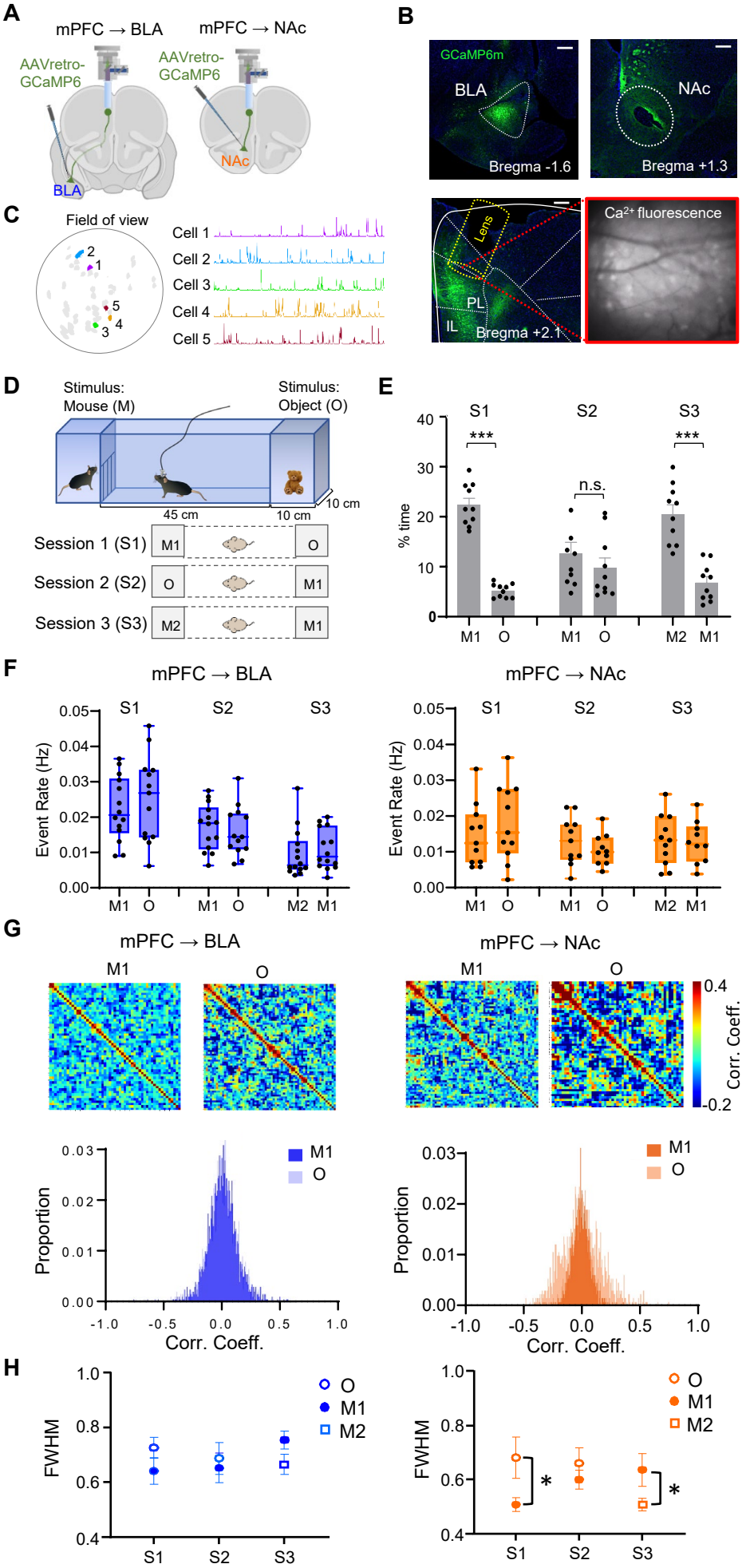
A
mPFC → BLA
mPFC → NAc
AAVretro-GCaMP6
AAVretro-GCaMP6
BLA
NAc
B
GCaMP6m
BLA
Bregma -1.6
NAc
Bregma +1.3
Lens
PL
IL
Bregma +2.1
Ca2+ fluorescence
C
Field of view
Cell 1
Cell 2
Cell 3
Cell 4
Cell 5
D
Stimulus: Mouse (M)
Stimulus: Object (O)
45 cm
10 cm
10 cm
Session 1 (S1)
Session 2 (S2)
Session 3 (S3)
M1
O
M2
E
S1
S2
S3
% time
n.s.
F
mPFC → BLA
mPFC → NAc
Event Rate (Hz)
G
mPFC → BLA
mPFC → NAc
Corr. Coeff.
Proportion
H
FWHM

Figure 1. Pattern decorrelation is shown by the mPFC→NAc neurons, but not mPFC→BLA neurons.

(A). Schematic showing retrograde AAV-GCaMP6 injection in the Nac and NLA, respectively. In vivo calcium imaging was performed in the mPFC neurons expressing GCaMP6 via miniscope.

(B). Top: An example of AAVretro-GCaMP6 injection and expression in the BLA and Nac, respectively. Bottom: An example of GCaMP6m expression in the mPFC with AAVretro-GCaMP6 injection in the NAc and an image of Ca2+ fluorescence recorded with miniaturized microscope. Green, GCaMP6m. Scale bars, 200 μm.

(C). Left: the field of view under a GRIN lens in one mouse with identified neurons numbered and colored. Right: fluorescence traces of example neurons marked in the above panel.

(D). Top: the apparatus for the social interaction test. The subject mouse is in the middle 45 cm-long chamber; the 10 cm end compartments contain different stimuli. Bottom: the three sessions of the social interaction test. In the first 10-minute test session (S1), a strange mouse (M1) and an object (O) were placed in the end chambers; session 2 (S2) used the same stimuli but swapped their positions; in session 3 (S3) a new mouse (M2) replaced O, so that the subject mouse must choose whether to interact with a familiar or strange mouse (M1 vs. M2).

(E). The percentage of time that mice (n = 10) spent interacting with stimuli in each session.

(F). The averaged calcium event rate when mice were engaged with different stimuli over the three sessions. n = 14 mice mPFC→BLA group; n = 11 for mPFC→NAc group. Data are represented as mean ± SEM. The event rates during interaction with M1 and O did not show statistical significance across all three sessions for both the mPFC→BLA and mPFC→NAc groups, two-way RM-ANOVA with Bonferroni–corrected post hoc comparisons.

(G). Top: raster plots of correlation coefficient of paired mPFC neurons during interactions with different stimuli, from a representative mouse in mPFC→BLA and mPFC→NAc group, respectively. Bottom: distribution of pair-wise Pearson correlation coefficients among these recorded mPFC neurons in responding to stimuli in each session. The blue and orange plots represent M1 interactions, while the lighter colors represent the interaction with the other stimulus (O).

(H). The averaged full width at half maximum (FWHM) of correlation coefficient distribution of individual mice in mPFC→BLA (n = 11) and mPFC→NAc (n = 10) group during interactions with different stimuli.

Data are represented as mean ± SEM. ***P < 0.001, *P < 0.05, two-way repeated measures analysis of variance (RM-ANOVA) with Bonferroni–corrected post hoc comparisons.

Fig. 2

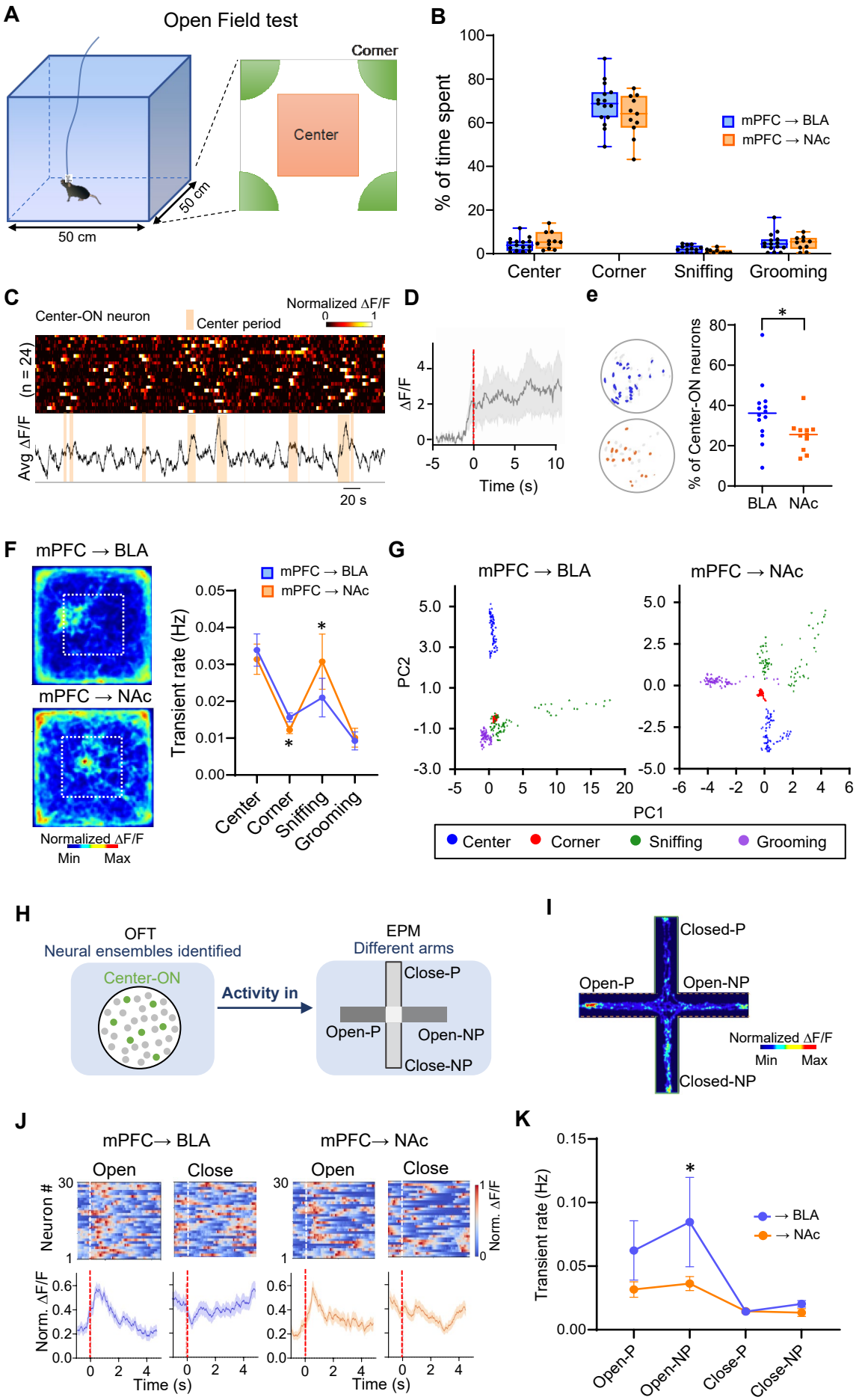
A
Open Field test
Corner
Center
50 cm
50 cm
B
% of time spent
mPFC → BLA
mPFC → NAc
Center
Corner
Sniffing
Grooming
C
Center-ON neuron
Center period
Normalized ΔF/F
(n = 24)
Avg ΔF/F
20 s
D
ΔF/F
Time (s)
e
% of Center-ON neurons
BLA
NAc
F
mPFC → BLA
mPFC → NAc
Transient rate (Hz)
Normalized ΔF/F
Min
Max
G
mPFC → BLA
mPFC → NAc
PC2
PC1
Center
Corner
Sniffing
Grooming
H
OFT
Neural ensembles identified
Center-ON
Activity in
EPM
Different arms
Close-P
Open-P
Open-NP
Close-NP
I
Closed-P
Open-P
Open-NP
Normalized ΔF/F
Min
Max
Closed-NP
J
mPFC→ BLA
mPFC→ NAc
Open
Close
Neuron #
Norm. ΔF/F
Time (s)
K
Transient rate (Hz)
→ BLA
→ NAc
Open-P
Open-NP
Close-P
Close-NP

Figure 2. The mPFC→NAc and mPFC→BLA neurons demonstrated distinct activity patterns across various emotional states.

(A) Schematic of the open field test (OFT) in an open 50 cm X 50 cm arena. The green areas represent corners and the orange area represents the center.

(B) The percentage of time that mice (n = 10) spent in the center, cornors, sniffing and grooming during 10-min open field test. n = 15 mice mPFC→BLA group; n = 11 for mPFC→NAc group. The behavioral performance between these two groups of mice showed no significant difference.

(C). Raster plots of individual neural activities and calcium traces of averaged group activity of center-ON neurons from one representative mouse in OFT. Vertical orange shadows indicate individual center epochs.

(D) Ca^{2+} traces of the averaged activity of center-ON neuron ensembles around the onset of center entry (5 s before to 5 s after). Solid lines represent the averaged value and shaded regions indicate SEM.

(E) Left: spatial distributions of center-ON neurons among the mPFC→BLA and mPFC→NAc neurons in one representative mouse from each group. Right: the percentage of center-ON neurons within the mPFC→BLA and mPFC→NAc neuron ensembles.

(F) Left: Mean Ca^{2+} signal across the open field arena of all observed center-ON neurons in one example mouse of mPFC→BLA and mPFC→NAc groups. The color bar indicates the averaged normalized z-score. Right: Averaged transient rate in four different states during the OFT.

(G) Sample distributions of the spatiotemporal features extracted by PCA analysis from two mice, each from a group.

(H). Analysis design of observing the neural activities of center-ON ensembles of OFT in different EPM arms.

(I). Mean Ca2+ signal across the EPM arms of all observed center-ON neurons in one example mouse. The color bar indicates the averaged normalized z-score.

(J). Example 30 center-ON neurons (top) and corresponding averaged activity (bottom) around the onset of arm entry during the EPM test. Time 0 represents the onset of arm entry.

(K) Averaged transient rate in four different arms during the EPM test. n = 9-13 mice mPFC→BLA group; n = 5-8 mice for mPFC→NAc group.

Data are represented as mean ± SEM. *P < 0.05, two-way RM-ANOVA with Bonferroni–corrected post hoc comparison.

Fig.3

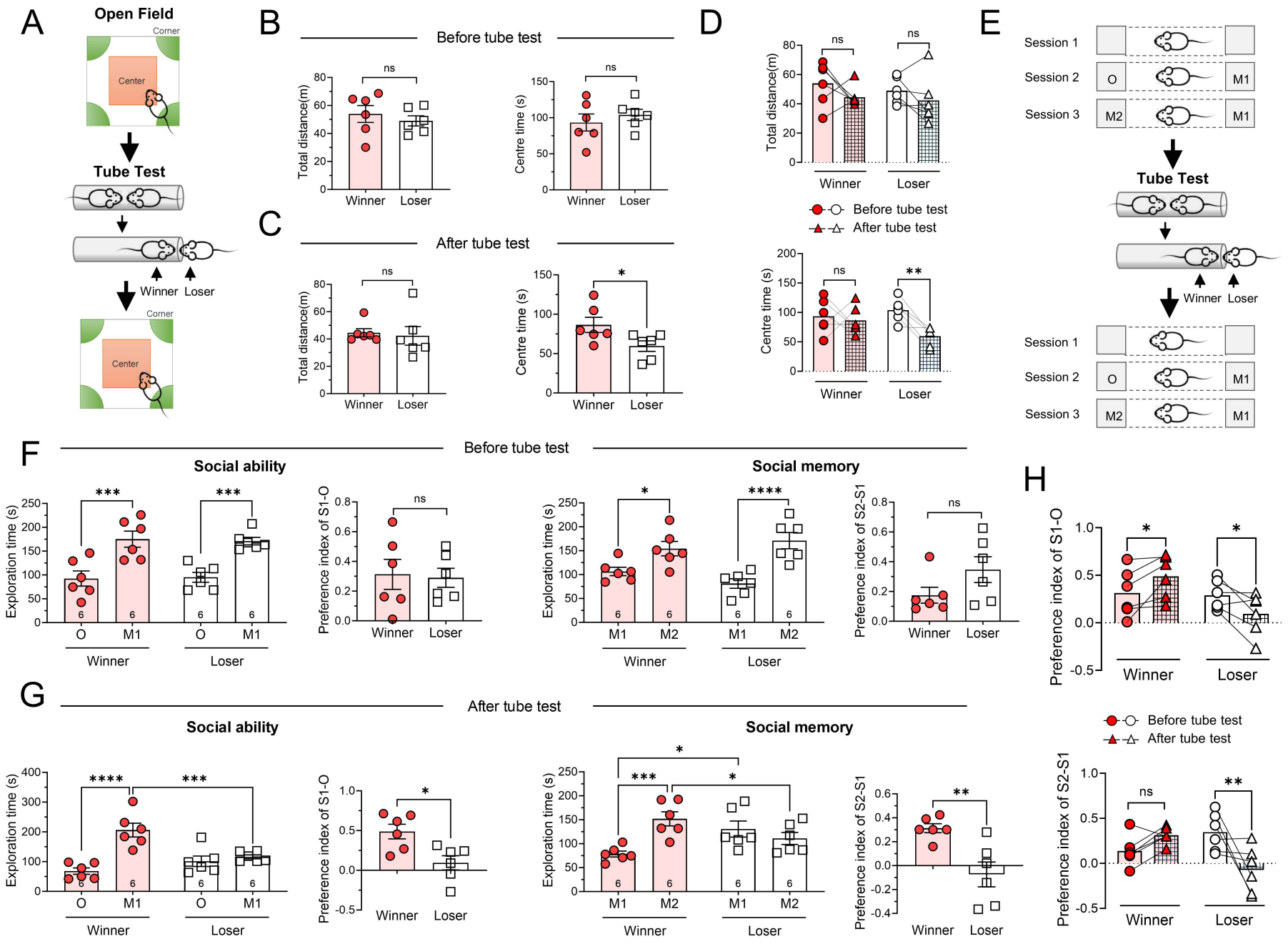
A
Open Field
Corner
Center
Tube Test
Winner
Loser
Corner
Center
B
Before tube test
Total distance(m)
Centre time (s)
ns
Winner
Loser
C
After tube test
Total distance(m)
Centre time (s)
ns
*
Winner
Loser
D
Total distance(m)
Centre time (s)
ns
**
Winner
Loser
Before tube test
After tube test
E
Session 1
Session 2
Session 3
O
M1
M2
Tube Test
Winner
Loser
F
Before tube test
Social ability
Social memory
Exploration time (s)
Preference index of S1-O
Preference index of S2-S1
***
*
****
ns
O
M1
M2
Winner
Loser
G
After tube test
Social ability
Social memory
Exploration time (s)
Preference index of S1-O
Preference index of S2-S1
****
***
*
**
ns
H
Preference index of S1-O
Preference index of S2-S1
Before tube test
After tube test
Winner
Loser

Figure 3. The modifications in social ranking of mice alter their anxiety and social states.

(A). Schematic illustrating the experimental scheme. Mice underwent an open field test, followed by five consecutive days of tube tests (once daily) to establish their social rankings. Subsequently, both the winner and loser mice underwent a repeat open field test to assess their anxiety states.

(B,C). The mice's total distance traveled in the open field and time spent in the center zones before and after the tube test. *P < 0.05; ns, non-significant. n = 6 mice for each group, winner vs loser, unpaired Student's t-test.

(D) The differences of total distance (top) and center time (below) between winner and loser groups before and after the tube tests. ***P < 0.0001; ns, non-significant. Before vs. after tube test, Two-way ANOVA Multiple comparisons, sidak's post-hoc test.

(E). Schematic illustrating the three-chamber test for social ability and social memory. Mice were introduced to the middle chamber, which comprised two smaller side chambers, and underwent three 10-minute sessions. In Session 1, mice acclimated to the apparatus without the presence of another mouse or object (O). For the social ability test (session 2), a novel mouse (M1) occupied one side chamber, while an object was placed in the other. In the social memory test (session 3), the previously encountered mouse (M1) remained in one side chamber, while a new mouse (M2) replaced the object in the other side chamber. After the three-chamber test, the mice underwent tube tests to establish their social rankings followed by a repeat three-chamber test to assess their social states.

(F). The mice's exploration time near to M1 and O/M2 during the social ability test (left) and social memory test (right) conducted before the tube test. Social ability index calculated as (time near M1 chamber - time near object chamber) / (time near M1 chamber + time near object chamber). Social memory index calculated as (time near M2 chamber - time near M1 chamber) / (time near M2 chamber - time near M1 chamber). *P < 0.05, ***P < 0.001, ****P < 0.0001, ns, non-significant. Two-way ANOVA Multiple comparisons, sidak's post-hoc test. Unpaired Student's t-test for preference index.

(G). The mice's exploration time spent near the M1 and O/M2 during social ability test and social memory test after the tube test. *P < 0.05, ***P < 0.001, ****P < 0.0001. Two-way ANOVA Multiple comparisons, sidak's post-hoc test. Unpaired Student's t-test for preference index.

(H). The comparisons of the social ability index (top) and social memory index (below) of winner and loser group before and after the tube tests. *P < 0.05, **P < 0.001, ***P < 0.001, ns, non-significant. Two-way ANOVA Multiple comparisons, sidak's post-hoc test). n = 6 mice for each group.

Fig. 4

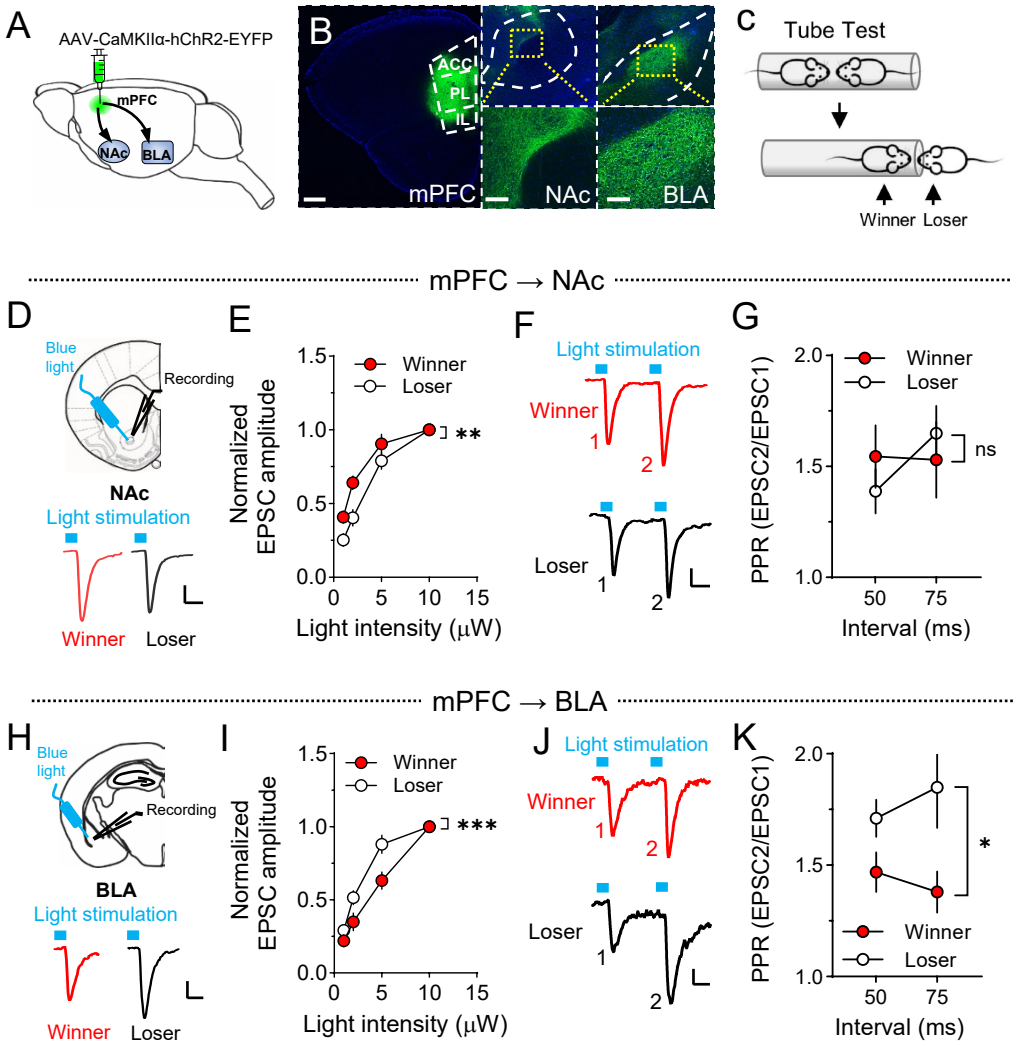

Figure 4. The social status dependent PL-NAc and PL-BLA neuronal activities.

(A). Schematic showing the AAV-ChR2 injection in the PL of mPFC.
(B). Expression of ChR2-EYFP in the mPFC, and terminal expression of ChR2-EYFP in the NAc and BLA. Scale bar, 400 μm, 50 μm, and 50 μm, from left to right.
(C). The ChR2-EYFP expressed mice underwent tube test to determine their winner and loser status.
(D). The EPSCs in the NAc were evoked by 470 nM blue light. Upper, schematic showing the light fiber placement and EPSC recording sites in the NAc; Lower, representative EPSCs in the brain slices from winner (red) and loser (black) mice. Scale bar, 30 pA and 25 ms.
(E). The normalized light intensity-dependent EPSCs. The data points were normalized to 10 μW and were shown as mean value. Winner, n= 19 neurons/ 7 mice; Loser n= 14 neurons/ 7 mice.
(F) The representative pair pulse ratio (PPR) of the EPSCs in the NAc (the light intensity were 1-2 μW and the interpulse interval were 50 and 75 ms). Scale bar, 8 pA and 25 ms.
(G) Summarized plots of the PPR under different interpulse intervals. Winner, n= 7 neurons/ 7 mice; Loser, n = 14 neurons/ 7 mice. ns, non-significant. Scale bar, 8 pA and 25 ms.
(H-I). EPSC recordings in the BLA. Winner, n = 17 neurons/ 7 mice; Loser n = 21 neurons/ 7 mice. Scale bar, 6 pA and 25 ms.
(J) The representative PPR of the EPSCs in the BLA.
(K) Summarized plots of the PPR under different interpulse intervals. Winner, n = 8 neurons/ 7 mice; Loser, n = 11 neurons/ 7 mice. Scale bar, 3 pA and 25 ms.

Data are shown as mean ± SEM. *P < 0.05, **P < 0.001, ***P < 0.0001. Two-way ANOVA

Different emotional states engage distinct descending pathways from the prefrontal cortex

Pan Xu[1,7 #], Gyeongah Park[2 #], Xiaoqian Sun[3 #], Qian Ge[2 #], Zhen Jin[2], Chien-Hsien Lai[1], Xiaojie Liu[4], Qingsong Liu[4], Rahul Simha[3], Chen Zeng[5], Jianyang Du[2,6 *], Hui Lu[1 *]

Supplemental information:

5 supplemental figures

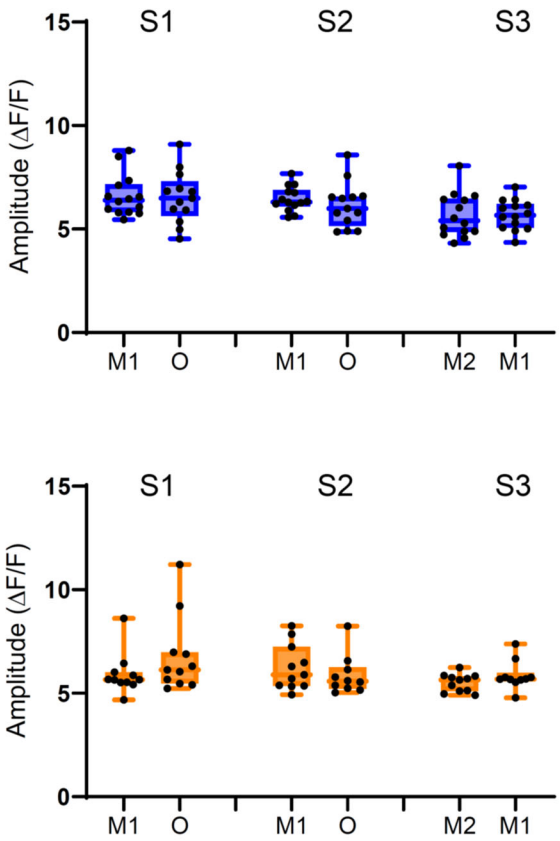

Supplementary Fig. S1. The amplitude of the mPFC→NAc and mPFC→BLA neurons showed no differences during social test. The averaged calcium transient amplitude when mice were engaged with different stimuli over the three sessions. n = 14 mice mPFC→BLA group; n = 11 for mPFC→NAc group.

Data are represented as mean ± SEM. Two-way ANOVA with Bonferroni–corrected post hoc comparisons. No significant difference was observed between the M1 and O or M2 and M1 in each group of mice.

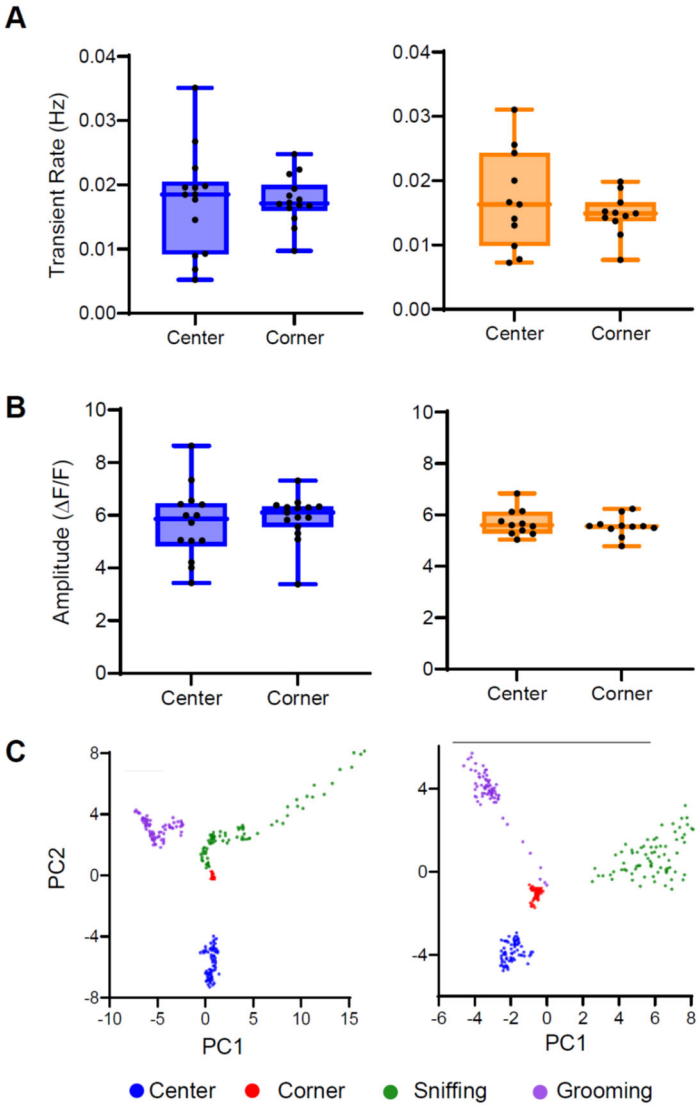

Supplementary Fig. S2. The activity pattern of all the recorded mPFC→NAc and mPFC→BLA neurons showed no differences during OFT.

(A,B) The averaged event rate (a) and amplitude (b) of the calcium transients when mice were in the center or corner of the open arena. n = 14 mice mPFC→BLA group; n = 11 for mPFC→NAc group. Data are represented as mean ± SEM. Two-way ANOVA with Bonferroni–corrected post hoc comparisons. No significant difference was observed between the center and corner in each group of mice.
(C) Distributions of the spatiotemporal features extracted by PCA analysis from two mice, each from a group.

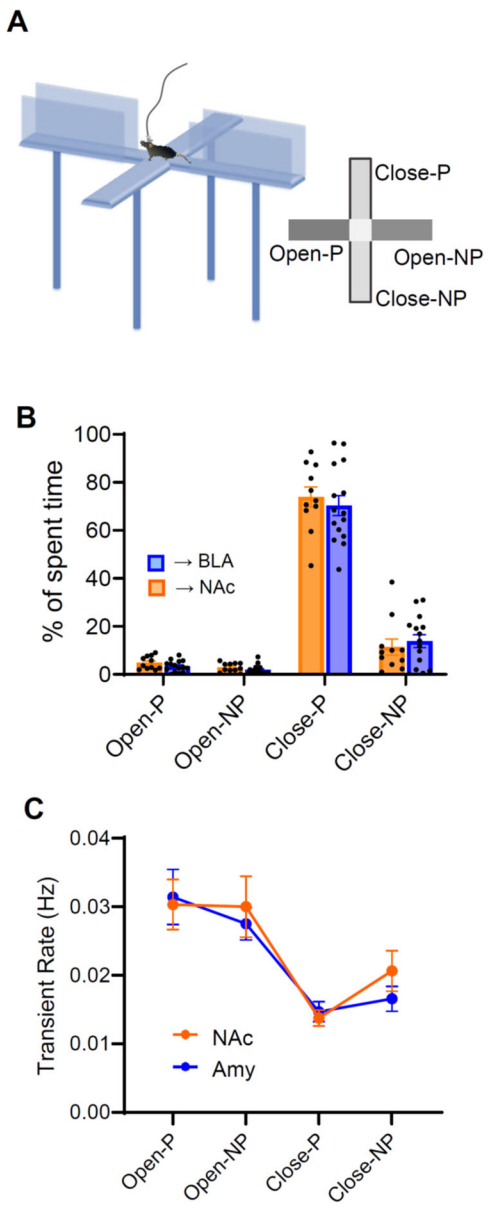

Supplementary Fig. S3. The activity pattern of all the recorded mPFC→NAc and mPFC→BLA neurons showed no differences during EPM test.

(A) Schematic of the elevated plus maze (EPM) test. The classification of the four arms is based on the duration of time that the mouse spends in each one. Open-P: preferred open arm; Open-NP: nonpreferred open arm; Close- P: preferred close arm; Close-NP: nonpreferred close arm.
(B). The percentage of time that mice spent in each arm during 10-min EPM test. n = 15 mice mPFC→BLA group; n = 11 mice for mPFC→NAc group.
(C) Averaged event rate of the calcium transients from all the recorded neurons in mPFC→NA and mPFC→BLA pathways. n = 9-13 mice mPFC→BLA group; n = 5-8 mice for mPFC→NAc group.

Data are represented as mean ± SEM. Two-way RM ANOVA with Bonferroni–corrected post hoc comparisons. No significant difference was observed for the two groups at each arm.

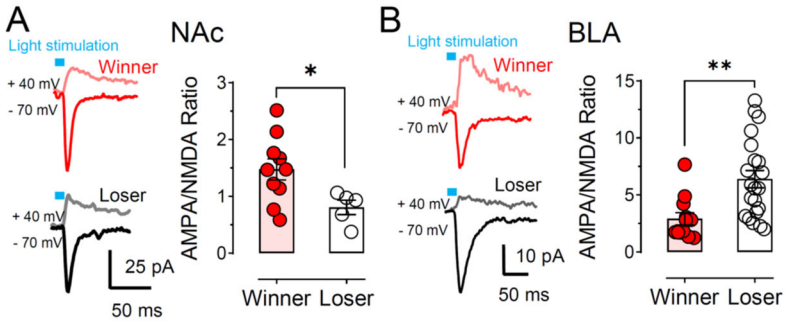

Supplementary Fig. S4. Social status alters AMAP/NMDA ratio in the PL-NAc and PL-BLA neurons.

(A) Left, representative EPSCs in the PL-NAc neurons from winner (red) and loser (black) mice. Right, the summarized AMAP/NMDA ratio. Winner, n= 5 neurons/ 5 mice; Loser n= 7 neurons/ 7 mice, 1-5 ms pulse). Scale bar, 25 pA and 50 ms.
(B) Left, representative EPSCs in the PL-BLA neurons from winner (red) and loser (black) mice. Right, the summarized AMAP/NMDA ratio. Winner, n= 12 neurons/ 7 mice; Loser n= 21 neurons/ 7 mice, 1-10 ms pulse). Scale bar, 10 pA and 50 ms.

Data are shown the as mean ± SEM. *P < 0.05, **P < 0.005 by two-tailed paired Student's t-test.

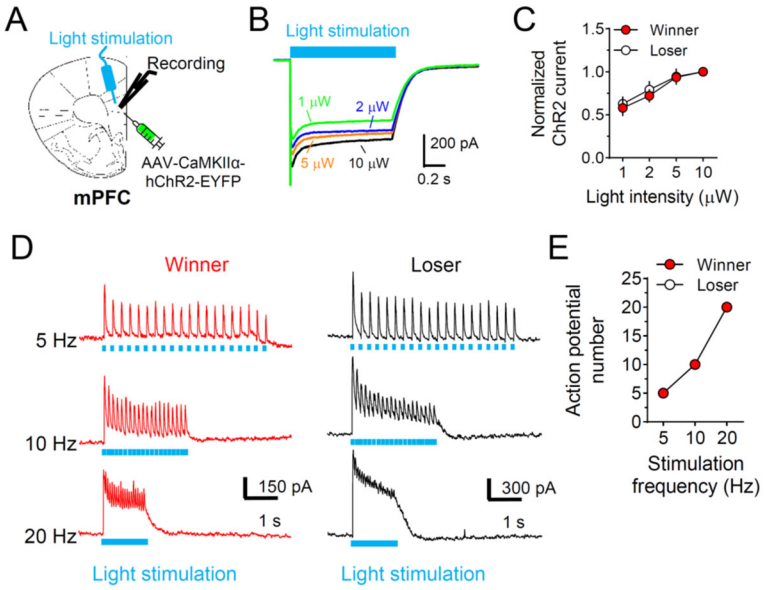

Supplementary Fig. S5. ChR2 currents in the PL neurons from the winner and loser mice.

(A) Schematic showing the light fiber placement and EPSC recording sites in the mPFC.
(B) The representative blue light intensity-dependent photocurrents.
(C) The normalized light intensity-dependent photocurrents in the neurons from winner (red) and loser (black) mice. Winner, n= 12 neurons/ 7 mice; Loser n= 16 neurons/ 7 mice.
(D) The representative traces of action potentials induced by blue lights.
(E) The summarized numbers of action potentials and the frequency of light stimulations. Winner, n= 7 neurons/ 4 mice; Loser n= 7 neurons/ 4 mice.

Data are shown the as mean ± SEM. Two-way ANOVA. No significant difference was observed between the winner and loser groups.